Halocline Internal Wave Attractors Visualization

Stepan Elistratov[1]

A Shirshov Institute of Oceanology of RAS
B Ivannikov Institute for System Programming of RAS
C Sobolev Institute of Mathematics of the Siberian Branch of the RAS

[1] ORCID: 0000-0002-7006-6879, sa.elist-ratov@yandex.ru

Abstract
The phenomenon of wave attractor, originating from ocean dynamics, in the last couple decades has become widely-studied both laboratorily and numerically. However, their discoveries in wild nature are still rare hence deepwater ones are out of technique, and attractor in smaller basins cannot form because of energy overinjection. In the current work we show that attractor may exist in shallower depths regardless the depth of the basin's bottom. Basing on the peculiar dispersion relation typical for stratified fluid attractors can be "trapped" in a narrow halocline layer which may facilitate their detection in the nature. Additionally, we discuss the formed flow structure visualization problems.

Keywords: wave attractor, visualization, CFD, fluid stratification, salinity profile.

1. Introduction

Wave attractor is a peculiar phenomenon of the flow motion concentration due to wave self-focusing in a specific geometry. As it was found [1], the necessary conditions for its formation are a slope side, periodic external forcing and density stratification along the gravity direction. Since the discovery of the phenomenon it became studied in laboratory tanks [2][3][4][5][6][7][8][9][10] as well as numerically [11][12][13][9][14][15], with divergence no more than 10% [11][16][12].

Despite the proposition in [1] that attractors may present in oceans and salt lakes, their observations in nature are still rare. One of the most demonstrative example is the investigation of wave attractor in Luzon Strait [17][18][19]. The deepwater attractor identification is difficult because of technically reasons, and as to those on shallower waters, their observation is obstructed by injected energy that turns out to be too large for attractor being stable [8].

Nonetheless, experiments and simulation were run for attractor with linear profile (former ones because of difficultness of salinity profile formation, latter ones tried to correspond the numerical setup). Such condition implies that attractor, if exists, forms through the entire depth. Numerical simulation allows to form any profile required, hence we tried to simulate a flow with internal wave attractor isolated by depth (existing only in a depth subrage). For attractor forms to meet dispersion relation

$$\omega/N = \sin\theta \tag{1}$$

where $N = \sqrt{-\frac{g}{\rho}\frac{\partial\rho}{\partial y}}$ is a buoyancy frequency, ω — wave frequency, θ — angle with the vertical direction, one may construct salinity profile that meets this condition only on certain depths. This will allow to modify attractor area regardless the basin shape. In this case, with a given external force, an attractor will be possible in a higher buoyancy frequency region which is situated where the salinity sharply increases, i.e. in halocline layer.

2. Numerical setup

As the computational domain we used trapezium-shaped area with one slope side (Fig. 1). In [1] is shown that the selection of this simple geometry is enough for an attractor formation. The numerical investigation can be a reliable for the numerical calculation [14][15] shows good convergence with the laboratory experiment [2][20].

One of the necessary conditions for wave attractor is a periodic forcing [1]. In order to provide it we reproduce a wave maker device [21] producing a border periodic perturbation with a given amplitude on a given frequency by a system of shafts and eccentrics [22][23], being placed on the top side (numerically we introduce it as a boundary condition). Two dimensional problem was solved following [16][11][12] hence it allows to save computational resources with a minimal lack of accuracy.
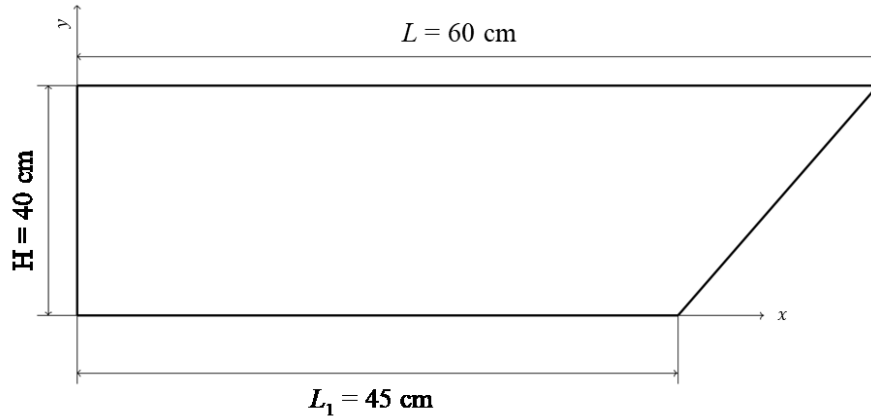
Figure 1: Problem domain

Mathematically the following equation describes the system: Navier-Stocks equation in Boussinesq approximation

$$\frac{\partial \vec{v}}{\partial t} + (\vec{v}, \nabla)\vec{v} = -\frac{1}{\rho_m}\nabla \tilde{p} + \frac{\rho_s}{\rho_m}\vec{g} \tag{2}$$

salt transition equation:

$$\frac{\partial \rho_s}{\partial t} + (\vec{v}, \nabla)\rho_s = \lambda_s \rho_s \tag{3}$$

$$\rho = \rho_m + \rho_s \tag{4}$$

and continuity equation (taking into account incompressibility):

$$\text{div } \vec{v} = 0 \tag{5}$$

Here $\tilde{p}$ is a presure without its hydrostatical part at ρ_m, ρ_m is a fresh water density, ρ_s — dissolved salt density, λ_s — salt diffusivity coefficient.

The x-axis is directed horysontally (alongside the trapezium base), y — vertically. The domain shape on Fig. 1.

The initial condition for velocity is zero:

$$\vec{v}|_{t=0} = \vec{0}$$

Wave maker was placed at the tope produces harmonic impact on a system via border oscillation:

$$s(x) = a\sin(\omega_0 t)\sin(2\pi x/L) \tag{6}$$

where $s(x)$ is an upper border profile, a and ω_0 are parameters.

As soon as the border displacement amplitude is much smaller than the domain height, the border profile condition (6) can be rewritten into a border velocity condition in a constant domain:

$$\vec{v}|_{y=H} \ = \ a\omega_0 \cos(\omega_0 t) \sin(\pi x/L)\vec{e}_y, \tag{7}$$

On the other borders we set $\vec{v}|_b = \vec{0}$

For the salinity the impermeability condition is used: $\frac{\partial \rho}{\partial n}$ on all the boundaries. For external force is periodic, we introduce a non-dimensional time t/T_0 ($T_0 \ = \ 1/f_0$). We ran our calculation with the same ω_0 external force frequency as for linear salinity profile. It is remarkable that we failed to determine attractor via ray-tracing method [2]. The problem was solved numerically using spectral element package *Nek5000* [24] providing high order of accuracy on a 48x48 spectral element grid with constant time step. For the postprocessing *python3* codes were utilized.

3. Salinity profiles & ray-tracing

To form the required attractor location we use the profiles depicted on Fig. 2-3.

The first (Fig. 2) profile with mid-depth halocline is more common for the northern basins [25][26], with a mid-depth profile inclination because of Atlantic water; the second one (Fig. 3) reproduces near-surface halocline as well as wind-mixed fresh water layer [27][28][29][30]. We emphasize that we did not followed the exact scales and reproduces only a qualitative features.
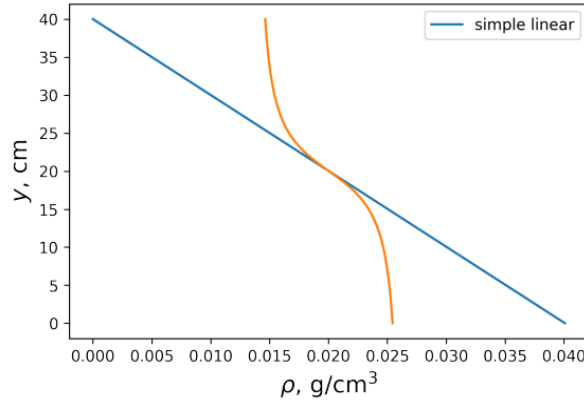
Figure 2: Mid-depth halocline profile vs linear
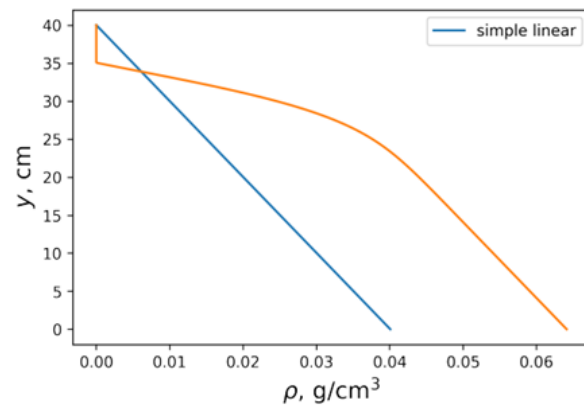
Figure 3: Shallow halocline profile vs linear

To make sure the attractor will form and to fit external frequency ω_0 we ran ray-tracing procedure [2]. It allow to follow the ray propagating according to dispersion relation 1. On the borders ray reflects so to maintain angle with vertical. As the density gradient is not constant, there can be zones where $\omega_0/N(y) > 1$, where ray cannot spreading because of sine range. If the ray meets such a zone, it also reflects. The attractor can be detected visually, if ray focuses and runs along the same trajectory many times.

For the selected geometry and different frequencies we make a diagram of attractor existence. All the attractors possible in the domain are hardly to be found at once, thus we concentrated on $(n, 1)$ type (n is a number of reflection from horizons, with only one vertical and slope reflection).
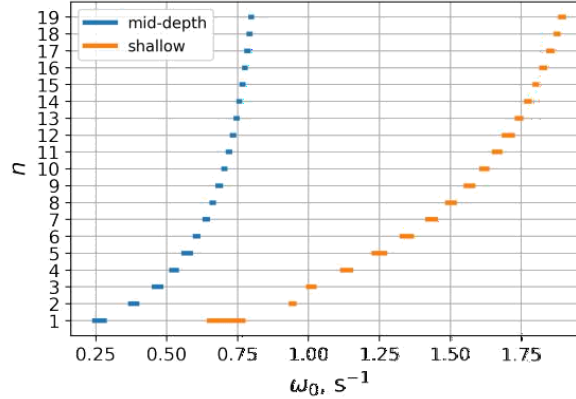
Figure 4: $(n, 1)$ attractors existence intervals for different halocline position

If the profile were linear, $(3, 1)$ would be the maximum (see [2], Fig. 2; slice $d = 0.5$). The profiles with halocline layers allow much more n. To comprehend the situation one must take into account that dispersion relation (1) imply that $\omega < N$, otherwise there is conventional seiche flow. As the salinity profile depends on vertical coordinate, for a given frequency inertial wave beams may propagate in one sub-region and not propagate in other; wherein they reflect from the layer(s) $y = y_0 \mid \omega = N(y_0)$ (we shall notice that it is a horizontal plane as N depends from y only. Becaus of this the attractor lives not in the whole domain but in a narrower subregion with greater aspect ratio, which allows the attractors $(n, 1)$ with greater n [31]. Moreover, for the salinity profiles selected (Fig. 2-3) it turns out that the higher is the frequency, the narrover is the attractor effective domain, and the higher n is possible. We plot attractors frequency intervals up to $n = 19$ for both profiles (Fig. 3).

We shall remember that ray-tracing prediction does not mean that attractor will appear in the liquid simulation — it may be destructed buy viscosity. To observe such structures we, on the one hand, would like to make it as narrow as possible, for attractor being really "trapped" in a small depths range, and on the other hand, we should maintain its height so that it will be visible despite viscous broading. We selected $(6, 1)$ type with frequencies 0.608 s^{-1} for the mid-depth halocline profile and 1.350 s^{-1} for the halocline one. The results of ray-tracing with these frequencies are represented on Fig.5-6.

Despite there is evident attractors, it doesn't mean we will find them in a numerical simulation. The point is that ray-tracing propose an infinitely thin attractor, but real attractor has its width which in fact depends on liquid viscosity: $\sigma \propto \nu^{1/3}$ [32]. The attractor on Fig. 6 has quite small edges, and to find the structure, we had to reduce the viscosity. It is not a cheat, because we solve the problem in a laboratory-size domain (60 cm× 40 cm) with the external force amplitude $a_0 = 0.002$ cm to yield a linear regime. As we suppose that such structures may present in ocean-scale basins, their scales will be much larger, and thus they may appear with a convertintional viscosity.
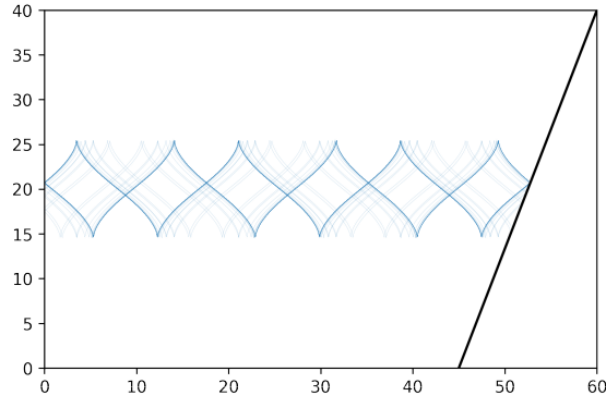
Figure 5: Ray-tracing, mid-depth halocline
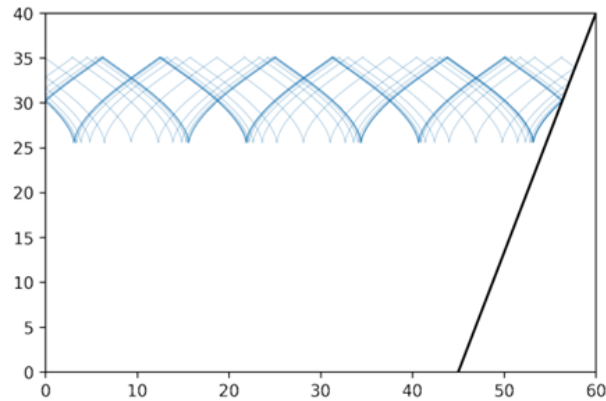
Figure 6: Ray-tracing, shallow halocline

To isolate attractor depthly we use high enough ω_0 for attractor lives in high-gradient area and can't live in that with low gradient. The high frequencies prohibit attractor from being very oblate (for it defines the angle with vertical, see (1)). That means that attractor cannot consist of only one rhomboid (so-called (1,1) attractor), and will have more than 1 reflection horizontally, or be $(n,1)$ attractor (see [31]).

4. Numerical simulation results visualization

4.1 Velocity

As a reference parameter we use vertical velocity components. Fig. 7-8 show "snapshots" of this variable. In terms of oceanology we are interested mostly in steady regime and less in the formation process, thus, snapshots are taken when the attractor structure is formed.

To follow the temporal evolution we consider v_y in dependence on t taken in a one particular point (Fig. 9-10, black mark). The oscillation and long time to steady regime establishing complicate the visualization, in contrary of the more ordinary full-sized (1,1) attractor [33].

At the beginning there is some transition process accompanied by oscillations' amplitude instability. We shall notice that amplitude steadifies (stops to increase, envelope becomes nearly constant) at the times far more that those of (1,1) attractor. It is not something surprising hence we dealt with $(n,1)$ attractor, and the higher the horizontal reflections number n, the greater the steadifying time [31].
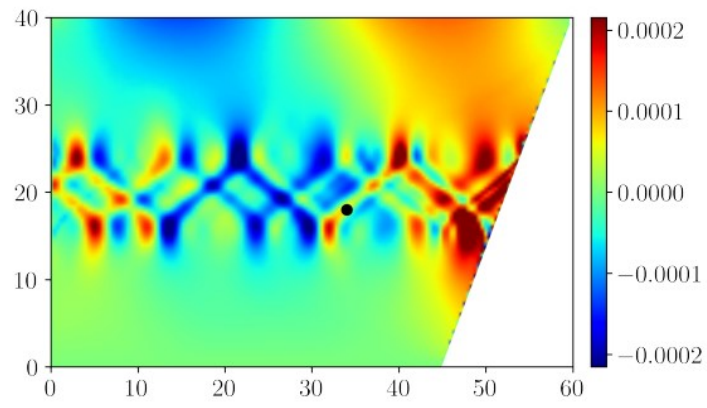
Figure 7: v_y snapshot, mid-depth halocline
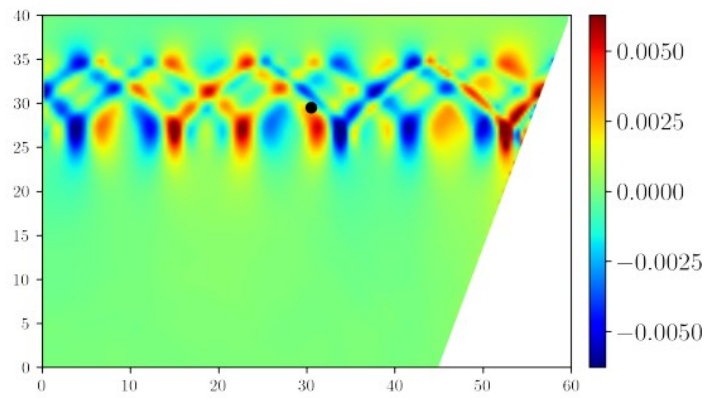
Figure 8: vy snapshot, shallow halocline
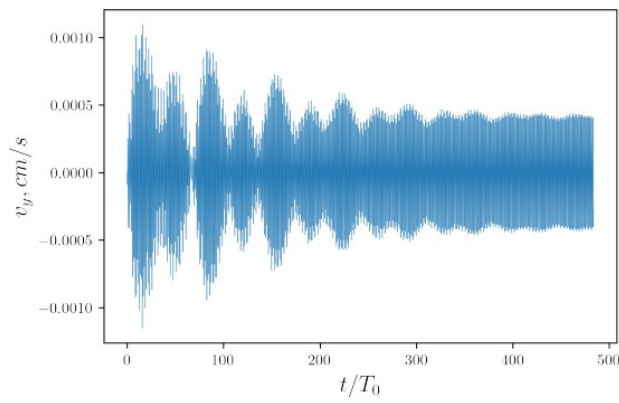
Figure 9: v_y evolution, mid-depth halocline
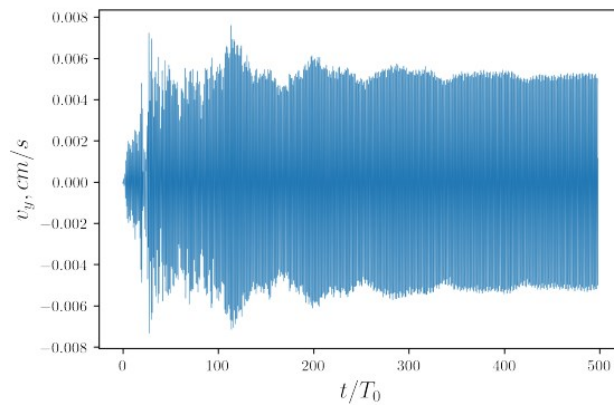
Figure 10: v_y evolution, shallow halocline

4.2. Velocity modulus

Hence the velocities oscillate, they can be of both positive and negative value (Fig. 9-10). This fact make an obstacle for the visual structure understanding, hence the attractor, if exists, will be of different color, which is seen on Fig. 7-8. It was not a problem for (1,1) attractor [33], it may be so in small-scaled attractor like the considered ones. To get rid of the oscillating colours and simultaneously take into account the other component, we plot velocity modulus on Fig. 11-12. It represents the structure quite well, except there are artifacts from the velocities of the area without attractors where the fluid moves in a seiche regime (upper part).
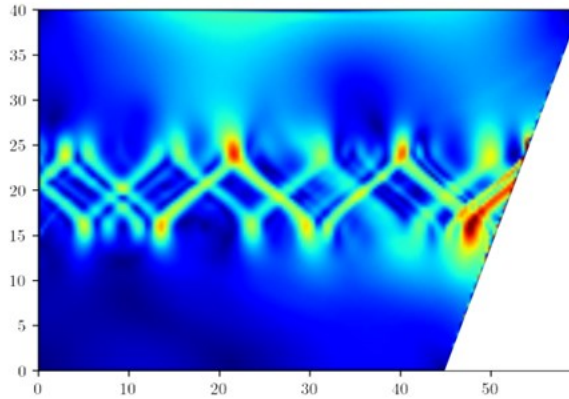
Figure 11: Velocity modulus, mid-depth halocline
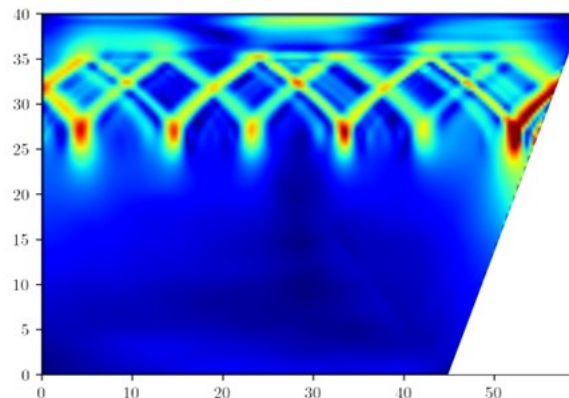
Figure 12: Velocity modulus, shallow halocline

4.3. Hilbert transform

The problem remaining is that the velocities in form of modulus still can oscillate, and the different hydrodynamical substructure may oscillate on different frequencies. To avoid this problem we propose to consider a velocity modulus Hilbert transform. For the oscillation functions it will yield an envelope.

The Hilbert transform shows a wave attractor structure better than pure velocity (13-14). At the same time, we shall say that the Hilbert envelope can also oscillate and in case of mid-depth halocline layer attractor required a precise selection of the time point which may be caused by a 'beat' instability (see Fig. 9). This method reveals almost no advantages in comparison with the simple velocity modulus plotting and made us to seek for different methods.
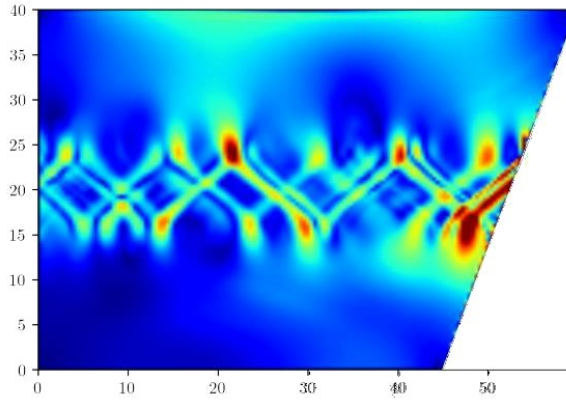
Figure 13: Velocity Hilbert transform, mid-depth halocline
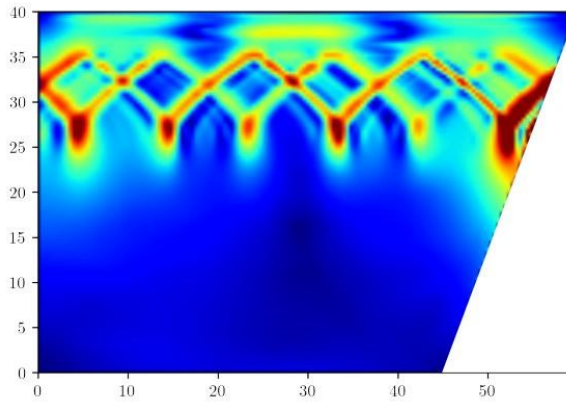
Figure 14: Velocity Hilbert transform, shallow halocline

4.4 Vortex identification

Another way for coherent structure identification is vortex identification methods. Despite the titled purpose — to represent vortices — some of them may help to visualize hydrodynamical structure. As it turns out, the better one in this sense is vorticity given by a simple formula:

$$\vec{\omega} = \text{ rot } \vec{v}$$

In three-dimensional case it is a vector whose direction is a local vortex axis, but as soon as our problem is 2D the vorticity is always orthogonal to the problem's plane, and there is a sense to consider only one component:

$$\omega_z = \frac{\partial v_y}{\partial x} - \frac{\partial v_x}{\partial y}$$

In the formulation given the method visualize a coherent structure quite well (Fig. 15-16). To be accurate we should say that hence the flow evolves in time, vorticity is calculated momentarily. However it turns out to be enough for attractor representation as the latter is seen clearly, but we emphasize that this structure is not so obvious under a default plot setting and requires a precise plotting tuning
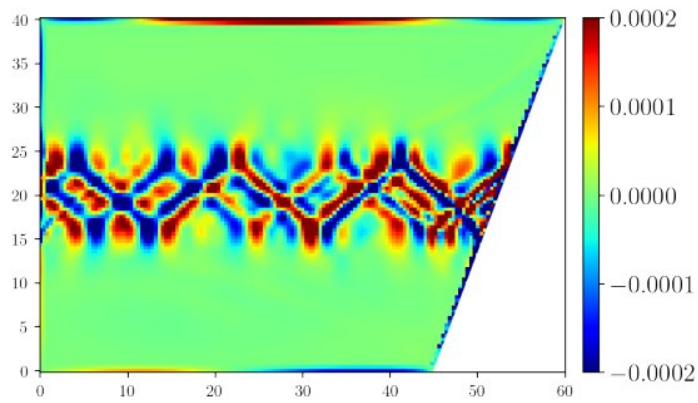
Figure 15: Vorticity, mid-depth halocline
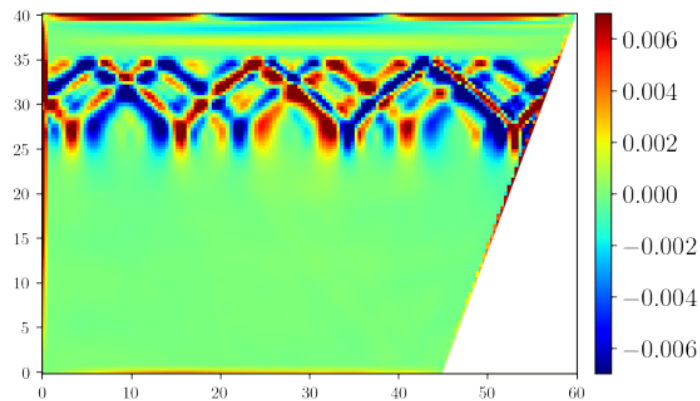
Figure 16: Vorticity, shallow halocline

Other methods of the vortex identification work with varying degrees of success. As an example we show widely-used Q-method on Fig. 17-18. In case of mid-depth halocline attractor it reveals some structure resembling that of the attractor, whereas being applied to the shallow halocline profile one it yields nothing intelligible. We do not recommend this method for attractors visualization because of such uncertainty of the results.
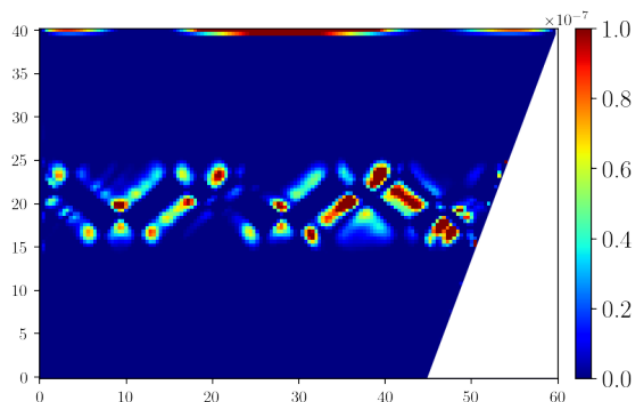
Figure 17: Q-criterion, mid-depth halocline
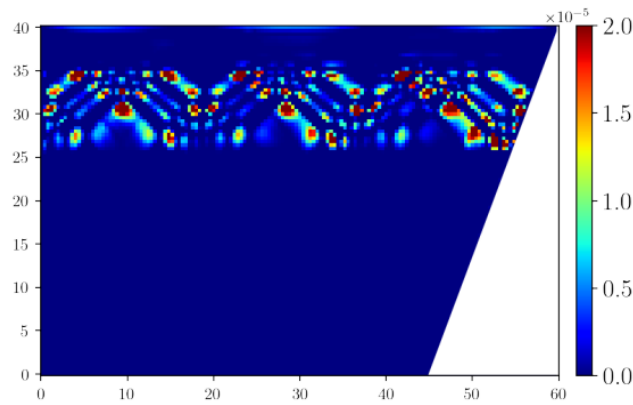
Figure 18: *Q*-criterion, shallow halocline

5. Conclusions and Discussions

Wave attractor natural observance is obstructed because of great energy input that demolishes the attractor structure and the necessity of wide-ocean scanning which requires special equipment and expensive on-vessel investigation. The full-depth attractros can form in places with a specific relief that also may complicate the problem.

Instead of full-depth sized attractors searching there is an option for attractors situated in a narrow depth range. We simulate the flow with certain salinity profiles which was close to real ones found in water basins. As the attractor rays widen because of viscosity, the smaller-cell attractor is visualized worse than a full-sized that is quite well representable by just a velocity component plotting, hence a narrow structure requires more complex techniques and more accurate plotting tuning.

Despite the difficulties with the visualization (and hence the detection if not deliberately simulated), this type of wave attractors — existing in a narrow depth range — may play not least role in the natural attractors detection. The tidal energy injection may distort the structure by the turbulence, but we hope with the proper visualization approach attractor may be founded in different basins.

References

1. Leo Maas and Frans-Peter A Lam. Geometric focusing of internal waves. *Journal of Fluid Mechanics*, 300:1–41, 1995.

2. L. R. M. Maas, D. Benielli, J. Sommeria, and F.-P. A. Lam. Observation of an internal wave attractor in a confined, stably stratified fluid. *Nature*, 388:557–561, August 1997.

3. Leo R. M. Maas. Wave focusing and ensuing mean flow due to symmetry breaking in rotating fluids. *Journal of Fluid Mechanics*, 437:13–28, 2001.

4. Astrid Manders and Leo Maas. Observations of inertial waves in a rectangular basin with one sloping boundary. *Journal of Fluid Mechanics*, 493:59–88, 2003.

5. Leo R.M. Maas. Exact analytic self-similar solution of a wave attractor field. *Physica D: Nonlinear Phenomena*, 238(5):502–505, 2009.

6. Jeroen Hazewinkel, Pieter Van Breevoort, Stuart B Dalziel, and Leo Maas. Observations on the wavenumber spectrum and evolution of an internal wave attractor. *Journal of Fluid Mechanics*, 598:373–382, 2008.

7. Arno Swart, Astrid Manders, Uwe Harlander, and Leo R.M. Maas. Experimental observation of strong mixing due to internal wave focusing over sloping terrain. *Dynamics of Atmospheres and Oceans*, 50:16–34, 2010.

8. H. Scolan, E. Ermanyuk, and T. Dauxois. Nonlinear Fate of Internal Wave Attrac-tors. *Physical Review Letters*, 110(23):234501, June 2013.

9. I. Sibgatullin, E. Ermanyuk, C. Brouzet, and T. Dauxois. Direct numerical simulation of attractors of internal gravity waves and their instability in stratified fluids. In

10. *International Summer Course and Workshop on Complex Environmental Turbulent Flows*, 2015.

11. Y. Dossmann, B. Bourget, C. Brouzet, T. Dauxois, S. Joubaud, and P. Odier. Mixing by internal waves quantified using combined PIV/PLIF technique. *Experiments in Fluids*, 57(8):132, August 2016.

12. Nicolas Grisouard, Chantal Staquet, and Ivane Pairaud. Numerical simulation of a two-dimensional internal wave attractor. *Journal of Fluid Mechanics*, 614:1–14, 2008.

13. C. Brouzet, T. Dauxois, E. Ermanyuk, S. Joubaud, M. Kraposhin, and I. Sibgatullin. Direct numerical simulation of internal gravity wave attractor in trapezoidal do-main with oscillating vertical wall. *Proceedings of the Institute for System Program-ming of the RAS*, 26(5):117–142, 2014.

14. Ogilvie G. I. Jouve L. Direct numerical simulations of an inertial wave attractor in lin-earand nonlinear regimes. *J. Fluid Mech.*, 745:223–250, 2014.

15. Christophe Brouzet, Ilias Sibgatullin, Helene Scolan, Evgeny Ermanyuk, and Thierry Dauxois. Internal wave attractors examined using laboratory experiments and 3d numerical simulations. *Journal of Fluid Mechanics*, 793:109–131, 2016.

16. Christophe Brouzet, Evgeny Ermanyuk, Sylvain Joubaud, Ilias Sibgatullin, and Thierry Dauxois. Energy cascade in internal-wave attractors. *EPL (Europhysics Letters)*, 113(4):44001, 2016.

17. Jeroen Hazewinkel, Nicolas Grisouard, and Stuart B Dalziel. Comparison of labora-tory and numerically observed scalar fields of an internal wave attractor. *European Journal of Mechanics-B/Fluids*, 30(1):51–56, 2011.

18. Antony Liu and Hsu Ming-Kuang. Internal wave study in the south china sea using synthetic aperture radar (sar). *International Journal of Remote Sensing*, 25:1261– 1264, 04 2004.

19. S. Cai, J. Xie, and J. He. An overview of internal solitary waves in the south china sea. *Acta Oceanologica Sinica*, (33):927–943, 2012.

20. Wang G., Zheng Q., Lin M., and Qiao F. Three dimensional simulation of internal wave attractors in the luzon strait. *Surv Geophys*, 34(11):14–21, 2015.

21. Christophe Brouzet, E Ermanyuk, Sylvain Joubaud, Grimaud Pillet, and Thierry Daux-ois. Internal wave attractors: different scenarios of instability. *Journal of Fluid Mechanics*, 811:544–568, 2017.

22. Gostiaux L., Didelle H., Mercier S., and Dauxois T. A novel internal waves genera-tor. *Experiments Fluids*, 42:123–130, 2007.

23. Mercier M.and Martinand D., Mathur M., Gostiaux L., Peacock T., and Dauxois T. New wave generation. *J. Fluid Mech.*, 657:308–334, 2010.

24. M. Mercier, N. Garnier, and T. Dauxois. Analyzing emission, reflection and diffrac-tion of internal waves using the Hilbert transform. In *APS Division of Fluid Dynam-ics Meeting Abstracts*, page G2, November 2008.

25. *https://nek5000.mcs.anl.gov/*.

26. Finlo Cottier, Frank Nilsen, R. Skogseth, Vigdis Tverberg, Jofrid Skardhamar, and H. Svendsen. Arctic fjords: A review of the oceanographic environment and dom-inant physical processes. *Geological Society of London Special Publications*, 344:35– 50, 11 2010.

27. Igor A. Dmitrenko, Sergey A. Kirillov, Bert Rudel, David G. Babb, Leif Toudal Ped-ersen, Søren Rysgaard, Yngve Kristoffersen, and David G. Barber. Arctic ocean outflow and glacier–ocean interactions modify water over the wandel sea shelf (northeastern greenland). *Ocean Sci.*, 45:1045–1060, 2017.

28. Sunny Jiang, W Fu, W Chu, and Jed Fuhrman. The vertical distribution and diver-sity of marine bacteriophage at a station off southern california. *Microbial ecology*, 45:399–410, 06 2003.

29. Derek Mueller, Patrick Hove, Dermot Antoniades, Martin Jeffries, and Warwick Vin-centb. High arctic lakes as sentinel ecosystems: Cascading regime shifts in climate, ice cover, and mixing. *Limnology and Oceanography*, 54, 11 2009.

30. Doo Lee, Keun-Hyung Choi, Ho Ha, Eun-Jin Yang, Sang Lee, SangHoon Lee, and Hyoung Chul Shin. Mesozooplankton distribution patterns and grazing impacts of copepods and euphausia crystallorophias in the amundsen sea, west antarctica, during austral summer. *Polar Biology*, 36, 07 2013.

31. I. Pasmans, A. Kurapov, J. Barth, A. Ignatov, P. Kosro, and R. Shearman. Why gliders appreciate good company: Glider assimilation in the oregon-washington coastal ocean 4dvar system with and without surface observations. *Journal of Geophysical Research: Oceans*, 124, 01 2019.

32. Ilias Sibgatullin, Alexandr Petrov, Xiulin Xu, and Leo Maas. On (n,1) wave attrac-tors: Coordinates and saturation time. *Symmetry*, 14(2), 2022.

33. C. Brouzet, I. N. Sibgatullin, E. V. Ermanyuk, S. Joubaud, and T. Dauxois. Scale effects in internal wave attractors. *Phys. Rev. Fluids*, 2:114803, Nov 2017.

34. D. A. Ryazanov, S.A. Elistratov, and M. V. Kraposhin. Visualisation for flows with internal waves attractors. *Scientific Visualization*, 13(5):113–121, 2021.